Electronic Structure of Ce-Doped and -Undoped Nd_2CuO_4 Superconducting Thin Films Studied by Hard X-Ray Photoemission and Soft X-Ray Absorption Spectroscopy

M. Horio,[1] Y. Krockenberger,[2] K. Yamamoto,[3] Y. Yokoyama,[3] K. Takubo,[3] Y. Hirata,[3] S. Sakamoto,[1] K. Koshiishi,[1] A. Yasui,[4] E. Ikenaga,[4] S. Shin,[3] H. Yamamoto,[2] H. Wadati,[3] and A. Fujimori[1]

[1]*Department of Physics, University of Tokyo, Bunkyo-ku, Tokyo 113-0033, Japan*
[2]*NTT Basic Research Laboratories, NTT Corporation, Atsugi, Kanagawa 243-0198, Japan*
[3]*Institute for Solid State Physics, University of Tokyo, Kashiwa, Chiba 277-8561, Japan*
[4]*Japan Synchrotron Radiation Research Institute, Sayo, Hyogo 679-5198, Japan*

(Received 25 October 2017; published 21 June 2018)

In order to realize superconductivity in cuprates with the T'-type structure, not only chemical substitution (Ce doping) but also postgrowth reduction annealing is necessary. In the case of thin films, however, well-designed reduction annealing alone without Ce doping can induce superconductivity in the T'-type cuprates. In order to unveil the origin of superconductivity in the Ce-undoped T'-type cuprates, we have performed bulk-sensitive hard x-ray photoemission and soft x-ray absorption spectroscopy on superconducting and nonsuperconducting $Nd_{2-x}Ce_xCuO_4$ ($x = 0$, 0.15, and 0.19) thin films. By postgrowth annealing, core-level spectra exhibited dramatic changes, which we attributed to the enhancement of core-hole screening in the CuO_2 plane and the shift of chemical potential along with changes in the band filling. The result suggests that the superconducting Nd_2CuO_4 film is doped with electrons despite the absence of the Ce substitution.

DOI: 10.1103/PhysRevLett.120.257001

High-temperature superconductivity in cuprates is realized by doping hole or electron carriers into the parent material, which has been widely considered to be an antiferromagnetic (AFM) Mott insulator. Ln_2CuO_4 (Ln is rare earth) with the T'-type structure, where Cu takes the square-planar coordination, can be doped with electrons by substituting Ce^{4+} for Ln^{3+}. Generally, electron doping by Ce substitutions alone cannot induce superconductivity in bulk crystals of the T'-type cuprates, and an additional procedure of postgrowth annealing in a reducing atmosphere is required [1]. Three distinct microscopic scenarios have been experimentally proposed for the role of the reduction annealing [2]: (i) removal of impurity apical oxygen atoms [3,4], (ii) creation of vacancies at the regular oxygen sites [5,6], and (iii) filling of Cu vacancies [7]. While the exact microscopic effect remains elusive, reduction annealing dramatically suppresses the AFM order [8,9] and reduces quasiparticle scattering [10], inducing superconductivity in the Ce-doped samples.

Furthermore, it has been demonstrated that thin films of T'-type cuprates can exhibit superconductivity without any Ce doping when properly annealed [11–14]. The observed decrease of the c-axis parameter by annealing [12–14] rather than its increase [7] should be attributed to the removal of apical oxygen atoms in these samples [3,4], as the removal of apical oxygen reduces the repulsion between the CuO_2 planes. The large surface-to-volume ratio of thin films helps the thorough removal of impurity oxygen atoms. The observation has cast doubt on the fundamental assumption that the parent compound of the cuprate superconductor is an AFM Mott insulator. Theoretical studies using the local density approximation plus dynamical mean field theory have indeed predicted that the parent compound of the T'-type cuprates is not a Mott insulator but a Slater insulator in the sense that the AFM order is necessary to open the insulating band gap [15–17]. When discussing the electronic structure of parent compounds and the phase diagram, however, the possibility should not be overlooked that oxygen reduction affects the carrier concentration. In fact, annealing-induced changes in the Néel temperature [18] and the optical conductivity [19] for bulk $Nd_{2-x}Ce_xCuO_4$ crystals have been interpreted as due to the doping of 0.03–0.05 electrons/f.u. Recent angle-resolved photoemission spectroscopy (ARPES) studies on Ce-doped bulk single crystals [9,20] and that on insulating Ce-undoped thin films [21] have also shown that the electron concentrations of annealed samples estimated from the Fermi surface area are larger than that expected from the Ce concentrations. To understand the cuprate phase diagram and the electronic states of the parent compounds, it is important to unveil the electron concentration of the superconducting (SC) and nonsuperconducting (non-SC) Ce-undoped T'-type cuprates.

For that purpose, systematic studies of thin film samples with various Ce concentrations and reduction or oxidization treatments are necessary. However, ARPES measurements on such thin films are hampered by the lack of an *in situ* ARPES measurement system combined with a

molecular beam epitaxy (MBE) apparatus for the T'-type cuprates, which makes ARPES-quality surfaces available. This is because ARPES is a surface-sensitive technique. In this Letter, we report on measurements of bulk-sensitive hard x-ray photoemission spectroscopy (HAXPES) and soft x-ray absorption spectroscopy (XAS) of SC and non-SC $Nd_{2-x}Ce_xCuO_4$ thin films annealed or oxidized under various atmospheres. By HAXPES, one can measure core-level shifts and hence the chemical-potential shift, which directly probes the doped electron concentration. By annealing Nd_2CuO_4, we observed dramatic changes in the core-level spectra, which can be explained by the strong modification of core-hole screening in the CuO_2 planes and by the chemical-potential shift caused by electron doping. The present results indicate the possibility that the SC Ce-undoped T'-type cuprates are doped with a significant amount of electrons.

$Nd_{2-x}Ce_xCuO_4$ ($x = 0$, 0.15, and 0.19) thin films with thicknesses of 200, 100, and 100 nm, respectively, were grown on $SrTiO_3$ (001) substrates by MBE. For Nd_2CuO_4, we prepared three kinds of films: as-grown, weakly annealed, and annealed films, among which only the annealed film showed superconductivity with $T_c = 25.0$ K. The T_c was defined as the temperature where the resistivity drops to zero. Ce-doped films showed superconductivity without *ex situ* annealing in a tubular furnace. The T_c's were 24.0 and 21.5 K for $x = 0.15$ and $x = 0.19$, respectively. Oxidized non-SC films were also prepared for both the compositions. Conditions of annealing and oxidization are described in Supplemental Material [22]. The resistivity curves and the c-axis lengths of all the films are plotted in Fig. 1. The difference in the c-axis length between the SC and non-SC films in Fig. 1(d) may largely originate from the difference in the amount of apical oxygen atoms [12–14].

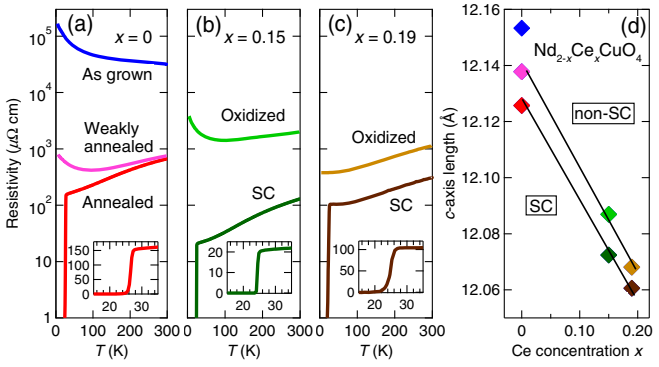

FIG. 1. Physical properties of $Nd_{2-x}Ce_xCuO_4$ thin films. (a)–(c) Resistivity versus temperature for the $x = 0$, 0.15, and 0.19 films, respectively. The insets show a magnified plot near the SC transition for each composition. (d) c-axis lengths plotted against Ce concentration x. The markers are color coded according to (a)–(c). Two solid lines trace the c-axis lengths of SC and non-SC films whose difference may originate from the different amount of apical oxygen atoms.

HAXPES measurements were performed at beam line 47XU of SPring-8 at $T = 300$ K with $h\nu = 7.94$ keV photons. The total energy resolution was determined from the Fermi edge of Au to be 0.3 eV. XAS measurements were performed in the total electron yield mode at beam line 07LSU of SPring-8 at $T = 300$ K under the pressure better than 5×10^{-9} torr. Two kinds of linearly polarized light, with polar angle $\theta = 90°$ ($\mathbf{E} \perp c$) and $\theta = 30°$, were used for the measurements [23].

Figure 2(a) shows Cu L_3-edge XAS spectra for $\mathbf{E} \| c$ and $\mathbf{E} \perp c$ for as-grown and annealed Nd_2CuO_4 films. The spectra for $\mathbf{E} \| c$ were obtained by subtracting the contribution of $\mathbf{E} \perp c$ from the spectra measured with $\theta = 30°$ polarization. The absorption intensity is proportional to the unoccupied density of states (DOS) of the specific element multiplied by transition matrix elements [30], which depends on the initial- and final-state orbital symmetry as well as incident light polarization. Thus, XAS provides information about the element- and orbital-specific unoccupied DOS. With polarization $\mathbf{E} \perp c$, the matrix element of the transition into the $3d_{x^2-y^2}$ orbital is 3 times larger than that into the $3d_{3z^2-r^2}$ orbital, while the polarization $\mathbf{E} \| c$ allows only the transition into the $3d_{3z^2-r^2}$ orbital (see Supplemental Material [22]). The XAS spectra for $\mathbf{E} \perp c$ show an intense peak at ~930 eV and its intensity decreases with annealing by 30%, suggesting the reduction of unoccupied DOS near the Fermi level (E_F) as reported for Ce-doped samples [31–34]. In contrast, spectra for $\mathbf{E} \| c$ remain negligibly weak. This leads to a small ratio of the $3d_{3z^2-r^2}$ weight to the $3d_{x^2-y^2}$ weight (4% and 2% for as-grown and annealed Nd_2CuO_4, respectively), in agreement with previous reports [32,33]. Therefore, the $3d_{3z^2-r^2}$ orbitals are almost completely filled regardless of whether annealed or not, and additional electrons go to the $3d_{x^2-y^2}$ orbitals by annealing. On the other hand, the preedge peak (~529 eV) in O K-edge XAS measured with $\mathbf{E} \perp c$ [Fig. 2(b)], which represents the transition from O $1s$ to in-plane O $2p$ orbitals hybridized with the upper Hubbard band, shows only a slight change (5%) in contrast to Cu $L_{2,3}$-edge XAS for $\mathbf{E} \perp c$. This agrees with the changes

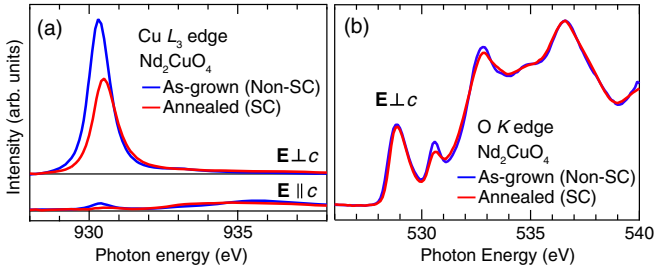

FIG. 2. XAS spectra of Nd_2CuO_4 thin films. (a) Cu L_3-edge XAS spectra for $\mathbf{E} \perp c$ (top) and $\mathbf{E} \| c$ (bottom) polarizations. The spectra have been normalized to the intensity of the Nd $M_{4,5}$ XAS peak at 978 eV. (b) O K-edge XAS spectra for $\mathbf{E} \perp c$ and normalized to the intensity at 532–540 eV.

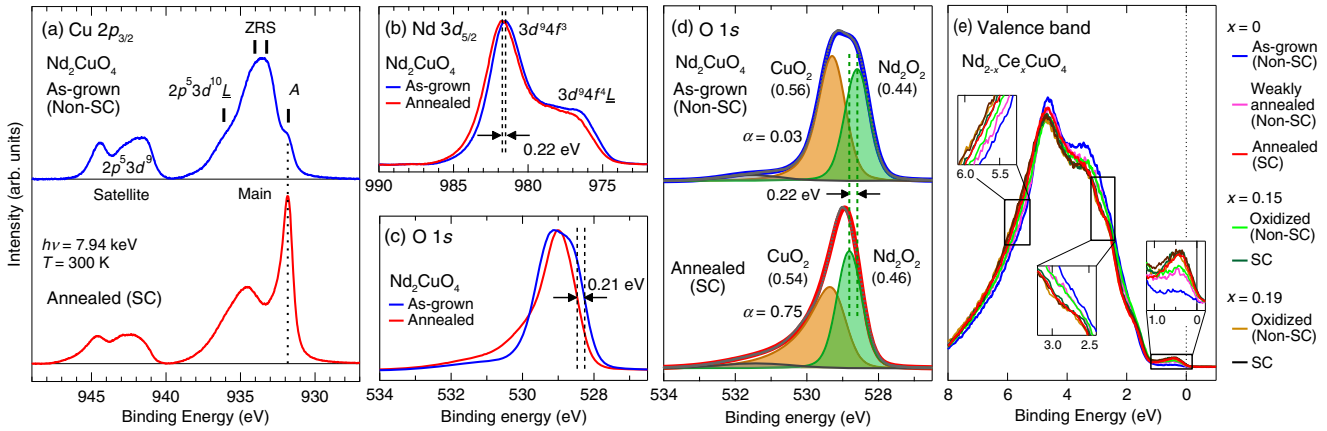

FIG. 3. HAXPES spectra of $Nd_{2-x}Ce_xCuO_4$ thin films. (a) Cu $2p_{3/2}$ core-level spectra of the as-grown non-SC (top) and annealed SC Nd_2CuO_4 thin films (bottom). One observes final states where the core holes are unscreened ($2p^53d^9$), screened by an electron transferred from neighboring oxygen atoms ($2p^53d^{10}\underline{L}$), screened by an electron transferred from neighboring CuO_4 plaquettes thereby creating a Zhang-Rice singlet (ZRS), and screened by conduction electrons (A). (b),(c) Nd $3d_{5/2}$ and O $1s$ core-level spectra normalized to the peak height, respectively, for the as-grown and annealed Nd_2CuO_4 films. (d) O $1s$ spectra of the as-grown (top) and annealed (bottom) Nd_2CuO_4 films fitted to a superposition of a Voigt function (for $O_{Nd_2O_2}$, green), a Mahan line shape $[1/\Gamma(\alpha)]\{[e^{-(E_B-E_0)/\xi}]/[|(E_B-E_0)/\xi|^{1-\alpha}]\}\Theta(E_B-E_0)$ convolved with a Voigt function (for O_{CuO_2}, orange), and another Voigt function (for O contamination, gray). Values in the parentheses represent the ratio of the peak area. (e) Valence-band spectra of $Nd_{2-x}Ce_xCuO_4$ thin films.

observed by Ce doping in the previous studies and suggests that the orbital character of the upper Hubbard band is dominated by $3d_{x^2-y^2}$ [31–33,35].

The effect of annealing is also remarkable in HAXPES spectra. Figure 3(a) shows the Cu $2p_{3/2}$ core-level HAXPES spectra of the as-grown and annealed Nd_2CuO_4 films. Upon photoemission from a core level, valence electrons are attracted to the core-hole site to screen its potential. Different types of core-hole screening result in various final states appearing as fine structures in the core-level photoemission spectra [36]. As has been discussed for the Cu $2p$ spectrum of insulating cuprates such as La_2CuO_4 [37,38] and $Sr_2CuO_2Cl_2$ [39,40] analyzed using multisite cluster calculation, the peak at the highest binding energy ($E_B = 940$–947 eV) is the satellite due to the $2p^53d^9$ final state with an unscreened core hole. In the main peak region ($E_B = 930$–939 eV), the highest binding energy peak corresponds to the $2p^53d^{10}\underline{L}$ final state, where an electron is transferred from the neighboring oxygen atoms (local screening) leaving a hole in the oxygen ligand orbital L, and the two peaks in the middle to the final state where an electron is transferred from oxygen in the neighboring CuO_4 plaquettes thereby creating a Zhang-Rice singlet in the plaquettes (nonlocal screening). Apart from peak A at the lowest binding energy discussed below, the line shape of the main peak resembles those of the other insulating cuprates with two-dimensional CuO_2 planes [40].

Upon annealing, peak A is strongly enhanced and the entire line shape dramatically changes. The binding energies of the charge-transferred final state are determined by the energy levels of the electronic states from which the electron is transferred to screen the core-hole potential. Therefore, the enhancement of the lowest energy peak indicates the development of electronic states closest to E_F [37,41] and is attributed to final states where the core hole is screened by conduction electrons. The observed changes in the present Cu $2p$ spectra therefore suggest that conduction electrons were introduced by annealing, consistent with the occurrence of superconductivity in the annealed Nd_2CuO_4.

The effect of annealing on the Nd and O core levels of Nd_2CuO_4 films is shown in Figs. 3(b)–3(d). Upon annealing, the Nd $3d_{5/2}$ peak was shifted toward higher binding energy by 0.22 eV [Fig. 3(b)]. As for the O $1s$ peak, a shift of similar amount (0.21 eV) was observed at the edge, but the spectral line shape is also modified: the full width at half maximum decreased from 1.44 to 1.16 eV and a long high binding energy tail emerges above ~529.5 eV [Fig. 3(c)]. Such changes have been overlooked in the doping and annealing dependence of the O $1s$ photoemission spectra of $Nd_{2-x}Ce_xCuO_4$ in previous studies [42,43]. In order to disentangle this complicated spectral deformation, the O $1s$ spectra have been analyzed as follows: The peak region of the O $1s$ spectrum of the as-grown film is rather flat, implying unresolved two peaks with similar intensities. We attribute them to oxygen atoms in the Nd_2O_2 layers ($O_{Nd_2O_2}$) and those in the CuO_2 planes (O_{CuO_2}), which are contained in Nd_2CuO_4 with equal amount. We calculated the oxygen binding energies using a WIEN2K package, and found that the $O_{Nd_2O_2}$ $1s$ level was located at a lower binding energy than the O_{CuO_2} $1s$ level [44]. Therefore, the O $1s$ spectra of the Nd_2CuO_4 films were fitted to a superposition of a Voigt function (for $O_{Nd_2O_2}$) at lower binding energies and Mahan line shape

$[1/\Gamma(\alpha)]\{[e^{-(E_B-E_0)/\xi}]/[|(E_B - E_0)/\xi|^{1-\alpha}]\}\Theta(E_B - E_0)$ convolved with a Voigt function (for O_{CuO_2}) at higher binding energies. The asymmetric Mahan line shape was assumed for O_{CuO_2} considering the core-hole screening by metallic electrons. Another Voigt function was added to the fitting function to reproduce a weak contamination component at ~531 eV. The fitting yielded $O_{Nd_2O_2}$ and O_{CuO_2} peaks with nearly the same area both for the as-grown and annealed films, as shown in Fig. 3(d), consistent with the initial assumption that each O 1s spectrum consists of two components arising from O_{CuO_2} and $O_{Nd_2O_2}$ [46]. The present analysis thus enables us to identify the effect of annealing on the two O 1s core levels separately: The $O_{Nd_2O_2}$ peak was shifted by 0.22 eV toward higher binding energy, and the O_{CuO_2} peak became strongly asymmetric (represented by the increase of asymmetry parameter α from 0.03 to 0.75). Since a finite DOS at E_F leads to a peak asymmetry, the strong asymmetry of the O_{CuO_2} peak in the annealed Nd_2CuO_4 film is consistent with the dramatic enhancement of the electrical conductivity. Another remarkable point is that annealing shifted the $O_{Nd_2O_2}$ 1s peak by almost the same amount as the Nd $3d_{5/2}$ peak without appreciable changes in the line shapes.

The shift of the core-level binding energy is given by [50]

$$\Delta E_B = \Delta\mu - K\Delta Q + \Delta V_M - \Delta E_R, \qquad (1)$$

where $\Delta\mu$ is the change in the chemical potential, ΔQ is the change in the number of valence electrons, K is a constant, ΔV_M is the change in the Madelung potential, and ΔE_R is the change in the extra-atomic screening of the core-hole potential by conduction electrons and/or dielectric polarization of surrounding media. Almost identical shifts observed for the Nd 3d and $O_{Nd_2O_2}$ 1s core levels indicate that ΔV_M is negligibly small because it would shift the core levels of the O^{2-} anion and the Nd^{3+} cation in different ways. ΔE_R cannot be the main origin of the observed shifts, either, because the increase of conduction electrons by annealing would shift the core-level peaks toward lower binding energy, opposite to the experimental observation. Considering that the valences of Nd^{3+} and O^{2-} are fixed ($\Delta Q = 0$), we conclude that the observed shifts in Nd 3d and $O_{Nd_2O_2}$ 1s core levels of Nd_2CuO_4 are largely due to the chemical potential shift $\Delta\mu$. The increase of the core-level binding energies by annealing indicates the increase of $\Delta\mu$ due to the addition of electrons.

Having identified the chemical-potential shift caused by annealing in Nd_2CuO_4, we compare the core-level structure of Nd_2CuO_4 with those of Ce-doped compounds. By Ce substitution, annealing, and oxidization, the Nd and Ce 3d spectra were shifted maintaining their shape. The lineshape changes in the Cu 2p and O 1s spectra were also consistent with the above scenario [51]. The chemical-potential shift $\Delta\mu$ defined as the average shift of the Nd 3d and $O_{Nd_2O_2}$ 1s core levels is plotted in Fig. 4(a) against Ce concentration x. For Nd_2CuO_4, the chemical potential is shifted upwards with annealing, reaching the level of Ce-doped $x = 0.15$ and 0.19 superconductors when sufficiently annealed. The valence-band spectra shown in Fig. 3(e) and Supplemental Material [22] are also almost identical among the three SC films with different Ce concentrations ($x = 0$, 0.15, and 0.19), indicating that the electronic structure and band filling are close to each other.

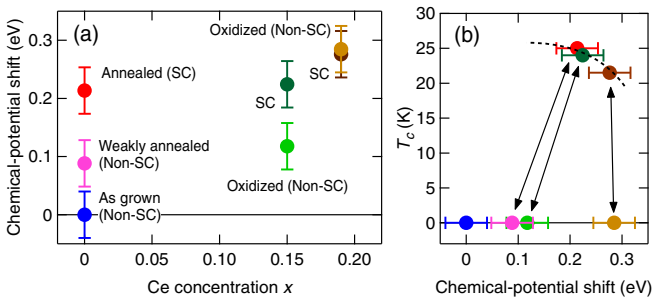

FIG. 4. Chemical-potential shifts in $Nd_{2-x}Ce_xCuO_4$ thin films. (a) Chemical-potential shifts $\Delta\mu$ defined as the average of the Nd 3d and O 1s core-level shifts plotted against Ce concentration x. (b) T_c's plotted against $\Delta\mu$. The markers are color coded according to (a). Thin films with shorter (longer) c-axis lengths and hence less (more) apical oxygen atoms are SC (non-SC) [see Fig. 1(d)]. The arrows connect the films with the same Ce concentration.

The large electron concentration for the annealed SC Nd_2CuO_4 film can be explained if oxygen atoms are removed not only from the apical site [3,4] but also from the regular sites (in the CuO_2 plane and/or the Nd_2O_2 layer) [5,6], leading to the total oxygen content less than the stoichiometric one. On the other hand, upon oxidization of $Nd_{2-x}Ce_xCuO_4$ ($x = 0.15$), chemical potential was shifted downwards, as can be seen in Fig. 4(a). This may be because the SC $x = 0.15$ film was already oxygen deficient and the vacancies were filled by oxidization. Consequently, the band filling of the T'-type cuprates is not determined by the Ce substitution alone but by the combined effect of Ce substitution and oxygen vacancies and, therefore, the phase diagram for this system should be made as a function of actual band filling, rather than as a function of Ce concentration. The oxidization process also introduced excess apical oxygen atoms, as suggested by the c-axis elongation [Fig. 1(d)], and the $x = 0.15$ film turned non-SC.

In Fig. 4(b), the T_c's of $Nd_{2-x}Ce_xCuO_4$ films are thus plotted against chemical-potential shift, which represents the electron concentration. The T_c values are not solely determined by the electron concentration since $x = 0.19$ films can be either SC or non-SC without a significant change in the electron concentration. The elongation of the c-axis lattice parameter by oxidization is also rather small for the $x = 0.19$ film (0.06%) compared to that for $x = 0.15$ film (0.12%), indicating that only a tiny amount

of apical oxygen atoms were incorporated. These results are consistent with previous studies where the amount of oxygen reduction decreases with increasing Ce concentrations [3,4,53]. The higher concentration of Ce^{4+} and the smaller c-axis lattice parameter may make the Ce-overdoped samples more robust against oxygen nonstoichiometry induced by reduction annealing and oxidization. While oxygen vacancy at the regular sites increases the electron concentration, excess oxygen atoms at the apical site immediately destroy superconductivity. The electronic structure of the T'-type cuprates are thus dominated not only by Ce concentrations but also by oxygen nonstoichiometry.

In conclusion, we have performed HAXPES and XAS measurements on $Nd_{2-x}Ce_xCuO_4$ ($x = 0$, 0.15, and 0.19) thin films with varying annealing atmosphere, and observed changes in the band-filling level among them. The electronic structure of SC Nd_2CuO_4 was found to be intimately linked to those of Ce-doped superconductors as the electrons were doped into the thin films by annealing probably through the creation of oxygen vacancies. Since the electron concentration and superconductivity of the T'-type cuprates are significantly affected by oxygen nonstoichiometry, the electronic structure should be discussed based on the actual electron concentration and oxygen occupancies rather than solely the Ce concentration.

Fruitful discussion with K. Okada and G. R. Castro is gratefully acknowledged. Experiments were performed at SPring-8 (Proposals No. 2015B1699, No. 2015B1793, No. 2015B7401, and No. 2016A1210). This work was supported by Grants-in-aid from the Japan Society of the Promotion of Science (JSPS) (Grants No. 14J09200 and No. 15H02109). M. H. acknowledges support from the Advanced Leading Graduate Course for Photon Science (ALPS) and the JSPS Research Fellowship for Young Scientists.

[1] Y. Tokura, H. Takagi, and S. Uchida, Nature (London) **337**, 345 (1989).
[2] N. P. Armitage, P. Fournier, and R. L. Greene, Rev. Mod. Phys. **82**, 2421 (2010).
[3] P. G. Radaelli, J. D. Jorgensen, A. J. Schultz, J. L. Peng, and R. L. Greene, Phys. Rev. B **49**, 15322 (1994).
[4] A. J. Schultz, J. D. Jorgensen, J. L. Peng, and R. L. Greene, Phys. Rev. B **53**, 5157 (1996).
[5] G. Riou, P. Richard, S. Jandl, M. Poirier, P. Fournier, V. Nekvasil, S. N. Barilo, and L. A. Kurnevich, Phys. Rev. B **69**, 024511 (2004).
[6] P. Richard, G. Riou, I. Hetel, S. Jandl, M. Poirier, and P. Fournier, Phys. Rev. B **70**, 064513 (2004).
[7] H. J. Kang, P. Dai, B. J. Campbell, P. J. Chupas, S. Rosenkranz, P. L. Lee, Q. Huang, S. Li, S. Komiya, and Y. Ando, Nat. Mater. **6**, 224 (2007).
[8] P. Richard, M. Neupane, Y.-M. Xu, P. Fournier, S. Li, P. Dai, Z. Wang, and H. Ding, Phys. Rev. Lett. **99**, 157002 (2007).
[9] M. Horio, T. Adachi, Y. Mori, A. Takahashi, T. Yoshida, H. Suzuki, L. C. C. Ambolode, K. Okazaki, K. Ono, H. Kumigashira, H. Anzai, M. Arita, H. Namatame, M. Taniguchi, D. Ootsuki, K. Sawada, M. Takahashi, T. Mizokawa, Y. Koike, and A. Fujimori, Nat. Commun. **7**, 10567 (2016).
[10] X. Q. Xu, S. N. Mao, W. Jiang, J. L. Peng, and R. L. Greene, Phys. Rev. B **53**, 871 (1996).
[11] A. Tsukada, Y. Krockenberger, M. Noda, H. Yamamoto, D. Manske, L. Alff, and M. Naito, Solid State Commun. **133**, 427 (2005).
[12] A. Tsukada, M. Noda, H. Yamamoto, and M. Naito, Physica (Amsterdam) **426C–431C**, 459 (2005).
[13] O. Matsumoto, A. Utsuki, A. Tsukada, H. Yamamoto, T. Manabe, and M. Naito, Physica (Amsterdam) **469C**, 924 (2009).
[14] Y. Krockenberger, H. Irie, O. Matsumoto, K. Yamagami, A. Tsukada, M. Naito, and H. Yamamoto, Sci. Rep. **3**, 2235 (2013).
[15] H. Das and T. Saha-Dasgupta, Phys. Rev. B **79**, 134522 (2009).
[16] C. Weber, K. Haule, and G. Kotliar, Nat. Phys. **6**, 574 (2010).
[17] C. Weber, K. Haule, and G. Kotliar, Phys. Rev. B **82**, 125107 (2010).
[18] P. K. Mang, O. P. Vajk, A. Arvanitaki, J. W. Lynn, and M. Greven, Phys. Rev. Lett. **93**, 027002 (2004).
[19] T. Arima, Y. Tokura, and S. Uchida, Phys. Rev. B **48**, 6597 (1993).
[20] D. Song, G. Han, W. Kyung, J. Seo, S. Cho, B. S. Kim, M. Arita, K. Shimada, H. Namatame, M. Taniguchi, Y. Yoshida, H. Eisaki, S. R. Park, and C. Kim, Phys. Rev. Lett. **118**, 137001 (2017).
[21] H. I. Wei, C. Adamo, E. A. Nowadnick, E. B. Lochocki, S. Chatterjee, J. P. Ruf, M. R. Beasley, D. G. Schlom, and K. M. Shen, Phys. Rev. Lett. **117**, 147002 (2016).
[22] See Supplemental Material at http://link.aps.org/supplemental/10.1103/PhysRevLett.120.257001 for sample preparation, XAS transition matrix elements, and more HAXPES spectra.
[23] See Supplemental Material at http://link.aps.org/supplemental/10.1103/PhysRevLett.120.257001 for more detailed experimental setup, which includes Refs. [24–29].
[24] H. Wadati and A. Fujimori, J. Electron Spectrosc. Relat. Phenom. **190**, 222 (2013).
[25] Y. Takata, M. Yabashi, K. Tamasaku, Y. Nishino, D. Miwa, T. Ishikawa, E. Ikenaga, K. Horiba, S. Shin, M. Arita, K. Shimada, H. Namatame, M. Taniguchi, H. Nohira, T. Hattori, S. Södergren, B. Wannberg, and K. Kobayashi, Nucl. Instrum. Methods Phys. Res., Sect. A **547**, 50 (2005).
[26] M. Sacchi, F. Offi, P. Torelli, A. Fondacaro, C. Spezzani, M. Cautero, G. Cautero, S. Huotari, M. Grioni, R. Delaunay, M. Fabrizioli, G. Vankó, G. Monaco, G. Paolicelli, G. Stefani, and G. Panaccione, Phys. Rev. B **71**, 155117 (2005).
[27] NIST Electron Inelastic-Mean-Free-Path database, Version 1.1, National Institute of Standard and Technology, 2000.
[28] S. L. Schroeder, Solid State Commun. **98**, 405 (1996).
[29] A. Ruosi, C. Raisch, A. Verna, R. Werner, B. A. Davidson, J. Fujii, R. Kleiner, and D. Koelle, Phys. Rev. B **90**, 125120 (2014).

[30] F. M. F. de Groot, J. C. Fuggle, B. T. Thole, and G. A. Sawatzky, Phys. Rev. B **42**, 5459 (1990).
[31] C. F. J. Flipse, G. van der Laan, A. L. Johnson, and K. Kadowaki, Phys. Rev. B **42**, 1997 (1990).
[32] E. Pellegrin, N. Nücker, J. Fink, S. L. Molodtsov, A. Gutiérrez, E. Navas, O. Strebel, Z. Hu, M. Domke, G. Kaindl, S. Uchida, Y. Nakamura, J. Markl, M. Klauda, G. Saemann-Ischenko, A. Krol, J. L. Peng, Z. Y. Li, and R. L. Greene, Phys. Rev. B **47**, 3354 (1993).
[33] J. Fink, N. Nücker, E. Pellegrin, H. Romberg, M. Alexander, and M. Knupfer, J. Electron Spectrosc. Relat. Phenom. **66**, 395 (1994).
[34] P. G. Steeneken, L. H. Tjeng, G. A. Sawatzky, A. Tanaka, O. Tjernberg, G. Ghiringhelli, N. B. Brookes, A. A. Nugroho, and A. A. Menovsky, Phys. Rev. Lett. **90**, 247005 (2003).
[35] A. Krol, C. S. Lin, Z. H. Ming, C. J. Sher, Y. H. Kao, C. L. Lin, S. L. Qiu, J. Chen, J. M. Tranquada, M. Strongin, G. C. Smith, Y. K. Tao, R. L. Meng, P. H. Hor, C. W. Chu, G. Cao, and J. E. Crow, Phys. Rev. B **42**, 4763 (1990).
[36] M. A. van Veenendaal and G. A. Sawatzky, Phys. Rev. Lett. **70**, 2459 (1993).
[37] M. Taguchi *et al.*, Phys. Rev. Lett. **95**, 177002 (2005).
[38] K. Maiti, J. Fink, S. de Jong, M. Gorgoi, C. Lin, M. Raichle, V. Hinkov, M. Lambacher, A. Erb, and M. S. Golden, Phys. Rev. B **80**, 165132 (2009).
[39] T. Böske, O. Knauff, R. Neudert, M. Kielwein, M. Knupfer, M. S. Golden, J. Fink, H. Eisaki, S. Uchida, K. Okada, and A. Kotani, Phys. Rev. B **56**, 3438 (1997).
[40] T. Böske, K. Maiti, O. Knauff, K. Ruck, M. S. Golden, G. Krabbes, J. Fink, T. Osafune, N. Motoyama, H. Eisaki, and S. Uchida, Phys. Rev. B **57**, 138 (1998).
[41] G. Panaccione, F. Offi, P. Torelli, G. Vanko, O. Tjernberg, P. Lacovig, A. Guarino, A. Fondacaro, A. Nigro, M. Sacchi, N. B. Brookes, and G. Monaco, Phys. Rev. B **77**, 125133 (2008).
[42] T. Suzuki, M. Nagoshi, Y. Fukuda, K. Oh-ishi, Y. Syono, and M. Tachiki, Phys. Rev. B **42**, 4263 (1990).
[43] N. Harima, J. Matsuno, A. Fujimori, Y. Onose, Y. Taguchi, and Y. Tokura, Phys. Rev. B **64**, 220507 (2001).
[44] See Supplemental Material at http://link.aps.org/supplemental/10.1103/PhysRevLett.120.257001 for details of calculation, which includes Ref. [45].
[45] J. C. Slater, Int. J. Quantum Chem. **5**, 403 (1971).
[46] See Supplemental Material at http://link.aps.org/supplemental/10.1103/PhysRevLett.120.257001 for more details about the fitting procedure, which includes Refs. [47–49].
[47] M. Ikeda, T. Yoshida, A. Fujimori, M. Kubota, K. Ono, H. Das, T. Saha-Dasgupta, K. Unozawa, Y. Kaga, T. Sasagawa, and H. Takagi, Phys. Rev. B **80**, 014510 (2009).
[48] R. Sankari, M. Ehara, H. Nakatsuji, Y. Senba, K. Hosokawa, H. Yoshida, A. D. Fanis, Y. Tamenori, S. Aksela, and K. Ueda, Chem. Phys. Lett. **380**, 647 (2003).
[49] P. H. Citrin, P. Eisenberger, and D. R. Hamann, Phys. Rev. Lett. **33**, 965 (1974).
[50] S. Hüfner, *Photoelectron Spectroscopy* (Springer-Verlag, Berlin, 1995), Chap. 2, p. 35.
[51] See Supplemental Material at http://link.aps.org/supplemental/10.1103/PhysRevLett.120.257001 for individual spectra, which includes Ref. [52].
[52] A. Kotani and Y. Toyozawa, J. Phys. Soc. Jpn. **37**, 912 (1974).
[53] K. Suzuki, K. Kishio, T. Hasegawa, and K. Kitazawa, Physica (Amsterdam) **166C**, 357 (1990).